THE JOURNAL OF PHYSICAL CHEMISTRY A
A JOURNAL OF THE AMERICAN CHEMICAL SOCIETY

pubs.acs.org/JPCA Article

Quantum State-Dependent Fragmentation Dynamics of D_2S Molecules Following Excitation at Wavelengths ∼ 129.1 and ∼ 139.1 nm

Published as part of The Journal of Physical Chemistry A special issue "Alec Wodtke Festschrift".

Zijie Luo, Shuaikang Yang, Yucheng Wu, Zhenxing Li, Wei Hua, Zhichao Chen, Li Che, Xingan Wang, Michael N.R. Ashfold,* Kaijun Yuan,* and Xueming Yang

Cite This: https://doi.org/10.1021/acs.jpca.4c04730 Read Online

ACCESS | Metrics & More | Article Recommendations | Supporting Information

ABSTRACT: The first high-resolution translational spectroscopy studies of D atom photoproducts following excitation to the Rydberg states of D_2S are reported. Excitation at wavelengths $\lambda \sim 139.1$ nm reveals an unusual 'inverse' isotope effect; the $^1B_1(3da_1 \leftarrow 2b_1)$ Rydberg state of D_2S predissociates much faster than its counterpart in H_2S. This is attributed to accidental near resonance with a vibrationally excited level of a lower-lying, more heavily predissociated Rydberg state of D_2S that boosts the probability of nonadiabatic coupling to the dissociation continuum with $^1A''$ symmetry. Excitation at $\lambda \sim 129.1$ nm populates the $^1B_1(4da_1 \leftarrow 2b_1)$ Rydberg state, which predissociates more slowly and allows the study of ways in which the branching into different quantum states of the SD products varies with the choice of parent excited (J_{KaKc}) level. All excited parent levels yield both ground (X) and electronically excited (A) state SD fragments. The former are distributed over a wide range of rovibrational (v'', N'') levels, while the population of levels with low v' and high N' is favored in the latter. These trends reflect the topographies of the dissociative $^1A''$ ($^1A'$) potential energy surfaces that correlate with the respective dissociation limits. Rotational motion about the *b*-inertial axis in the excited state molecule increases the relative yield of SD(A) products, consistent with dissociation by rotationally (Coriolis-) induced coupling from the photoexcited Rydberg level to the $^1A'$ continuum. Molecules excited to the rotationless ($J_{KaKc} = 0_{00}$) level also yield some SD(A) products, however, confirming the operation of a rival fragmentation pathway wherein photoexcited molecules decay by initial vibronic coupling to the $^1A''$ continuum, with subsequent nonadiabatic coupling between the $^1A''$ and $^1A'$ continua enabling access to the D + SD(A) limit.

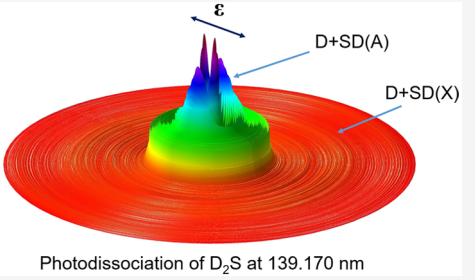

1. INTRODUCTION

Photodissociation following the absorption of ultraviolet (UV) light is an important destruction process for many small molecules in low density regions of the interstellar medium (ISM). Hydrogen sulfide (H_2S) has been detected in cometary coma,[1−5] in planetary atmospheres,[6−9] in protoplanetary disks in Taurus,[10] in an isolated massive protostar,[11] and in a brown dwarf.[12] The presence of H_2S in the hotter, denser atmosphere of the exoplanet Wasp-39b was inferred via detection of SO_2, at least some of which is attributed to photochemical processing of H_2S.[13] Now, H_2S has been detected directly in the atmosphere of the hot Jupiter HD189733B, with an abundance that suggests it is the main reservoir for sulfur in that environment.[14] Singly and doubly deuterated hydrogen sulfides have been detected in a few dark clouds, with a significant fractionation ratio of ∼0.1, but not in hot cores, even when the H_2S column densities were large.[15] High D/H fractionation ratios in gas phase species in the ISM are typically now reconciled by assuming release (by sputtering, thermal and/or photoinduced desorption) of material formed on grain surfaces during the cold, prestellar core phase, when the CO-depleted gas possessed large atomic D/H ratios.[16,17]

The present study focuses on D_2S photodissociation following excitation of two strong transitions at wavelengths $\lambda \sim 139.1$ and ∼ 129.1 nm. As Figure 1 shows, the electronic spectrum of D_2S exhibits two broad absorption regions. One, which maximizes at $\lambda \sim 195$ nm and extends into the near UV region, shows diffuse resonance structure.[18] Photoexcitation within this long wavelength band results in DS−D bond fission, yielding D atoms and ground-state SD(X) radicals.[19] Recent wavepacket calculations employing state-of-the-art potential energy surfaces (PESs) for the ground ($\tilde{X}^1A_1$) and

Received: July 15, 2024
Revised: August 27, 2024
Accepted: August 27, 2024

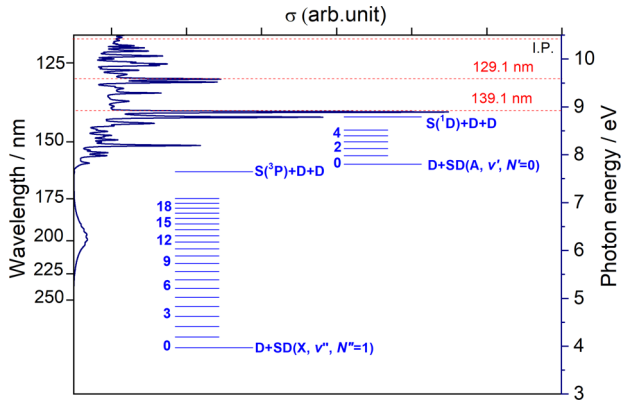

Figure 1. D_2S absorption cross-section σ versus wavelength (after ref 18, with the λ = 129.1 and 139.1 nm features highlighted, along with the energetic thresholds for each of dissociation channels I–IV, for ionization (I.P.) and for forming D atoms together with X and A state SD products in different v levels.

first two (strongly coupled) singlet excited states – both of $^1A''$ symmetry once the molecule starts to stretch asymmetrically – provide a detailed picture of the fragmentation dynamics.[20,21]

A second region of continuous absorption is evident at vacuum UV (VUV) wavelengths λ < 150 nm, lying beneath many intense, sharp features.[18,22−24] The underlying absorption is associated with excitation to a higher energy continuum of $^1A'$ symmetry, while the sharp peaks arise from excitations to Rydberg states belonging to series that converge to the first ionization potential of D_2S (IP = 84466 ± 2 cm^{-1} (ref 24)). The peaks at $\lambda \sim$ 139.1 and $\sim$ 129.1 nm are assigned as, respectively, the n = 3 and 4 members of a Rydberg series formed by electron promotion from the $2b_1$ highest occupied molecular orbital (HOMO) – essentially the S $3p_x$ orbital – to nda_1 Rydberg orbitals.[24] The HOMO and the Rydberg orbitals are all essentially nonbonding orbitals. The electron promotion thus causes negligible geometry change, and Franck–Condon considerations dictate that the absorption to each of these Rydberg states will be dominated by the v'=0 ← v''=0 origin band. Many of the Rydberg states have sufficient lifetimes (*i.e.*, predissociate sufficiently slowly) that their spectra show resolved rotational fine structure,[22−26] the analysis of which confirms the $^1B_1$ symmetry of the excited states responsible for the $\lambda \sim$ 139.1 and $\sim$ 129.1 nm bands.[24,27,28]

The number of possible photofragmentation pathways increases with an increase in excitation energy. The recent literature contains several photofragment translational spectroscopy (PTS) studies following excitation of H_2S at λ < 150 nm, monitoring both H and S atom photoproducts. These include free electron laser (FEL) enabled 'global' photolysis studies at many different excitation energies up to the first IP,[29−31] and higher resolution studies that explore how the fragmentation dynamics vary with parent rotational level following excitation to the two aforementioned predissociating Rydberg states with $^1B_1$ symmetry.[32,33] The former confirmed formation of $S(^1D)$ and $S(^1S)$ atoms in tandem with rovibrationally excited H_2 products but also showed both to be minor channels. HS–H bond fission is the dominant process at all wavelengths, and the relative yield of electronically excited SH(A) products increases rapidly once λ < 150 nm. The SH(A) fragments have a short (few nanoseconds at most) lifetime with respect to predissociation,[34] yielding a second H atom and a ground state $S(^3P)$ atom.[35−37] Most H_2S molecules excited at wavelengths shorter than ~130 nm undergo initial dissociation to H + SH(A) products en route to eventual 2H + $S(^3P)$ products.[29]

The rovibronically state resolved studies showed that the primary SH(A)/SH(X) product ratio following excitation to the $^1B_1$ states of H_2S responsible for $\lambda \sim$ 139.1 nm and ~ 129.1 nm absorption features scale with $\langle J_b^2 \rangle$, the expectation value of the square of the rotational angular momentum about the b-inertial axis in the photoexcited asymmetric top molecule.[32,33] The most straightforward explanation for this observation is that b-axis rotational motion has the appropriate symmetry to enable nonadiabatic (Coriolis) coupling from a state of $^1B_1$ symmetry to the background $^1A'$ continuum, which correlates with H + SH(A) products. This decay process is in competition with a rival (nonrotationally driven) vibronic channel, that enables nonadiabatic coupling from the photoprepared $^1B_1$ states to the lower-lying $^1A''$ continuum and eventual dissociation to H + SH(X) products.[31] However, the high-resolution PTS studies following excitation of H_2S within the 129.1 nm band found some SH(A) products from dissociating levels with $\langle J_b^2 \rangle$ = 0, implying that this explanation is incomplete.[33]

In contrast to the extensive investigations of H_2S, PTS studies of the heavier isotopomer, D_2S, at short UV photolysis wavelengths are rare – limited to just the D Lyman-α wavelength (λ = 121.534 nm, corresponding to a wavenumber of 82281.5 cm^{-1}).[19,38] Consistent with the analogous H_2S photolysis studies, D_2S photodissociation was shown to yield D atoms along with very highly rotationally excited SD(A) partners. Again, as with H_2S at such short wavelengths, the study showed that the forces that drive opening of the ∠DSD bond angle on the $^1A'$ PES(s) were sufficiently strong to yield some SD(A) fragments in 'super-rotor' levels, *i.e.*, in quasi-bound rotational levels above the thermochemical threshold for dissociation to D + $S(^1D)$ products. Such levels exist only by virtue of the accompanying centrifugal potential energy barrier. In the limit, such forces also lead to some three-body dissociation. The threshold energy for this process (IV) and the various other spin-allowed fragmentation channels of D_2S molecules that yield D atoms are listed in Table 1. Most SD(A) fragments from D_2S photolysis (process II in Table 1) predissociate, albeit less rapidly than in the case of SH(A) fragments, to the ground state atoms.[34−37] The threshold energies for channels I through IV are also included in Figure

Table 1. Thermochemical Threshold Energies (in cm^{-1}) for Spin-allowed Fragmentation Channels Yielding D Atoms (Channels I–IV) from D_2S, Derived Using Literature Values for the Bond Dissociation Energies $D_0°$(DS–D) [39] and $D_0°$(S–D) [37] and for the Atomic Level Separation $\Delta E(S(^1D_2–^3P_2))$,[40] and the Spectroscopically Determined Separation Between the $A^2\Sigma$, v' = 0, N' = 0, J' = 0.5 and $X^2\Pi_{3/2}$, v'' = 0, N'' = 1, J'' = 1.5 Levels of the SD Radical.[41]

channel	fragments	threshold energy/ cm^{-1}
I	D + SD($X^2\Pi_{3/2}$, v'' = 0, N'' = 1)	31999 ± 17
I′	SD($X^2\Pi_{3/2}$, v'' = 0, N'' = 1) → D + $S(^3P_2)$	29650 ± 20
II	D + SD($A^2\Sigma$, v' = 0, N' = 0)	62947 ± 17
II′	SD($A^2\Sigma$, v' = 0, N' = 0) → D + $S(^1D_2)$	7940 ± 20
III	D + D + $S(^3P_2)$	61649 ± 26
IV	D + D + $S(^1D_2)$	70888 ± 26

https://doi.org/10.1021/acs.jpca.4c04730
J. Phys. Chem. A XXXX, XXX, XXX–XXX

1, along with the energies of different vibrational levels of the SD(X) and SD(A) products.

Here, we present high resolution D atom PTS data following excitation to the $^1B_1$ states of D_2S populated by absorption at $\lambda \sim 129.1$ and ~ 139.1 nm. The study at the shorter wavelength allows a high level of parent rotational (*i.e.*, J_{KaKc}') level selection and thus detailed investigation of ways in which the fragmentation dynamics are influenced by the parent rotational angular momentum. The latter excitation is found to be much less well resolved, *i.e.*, the $^1B_1(3da_1 \leftarrow 2b_1)$ state of D_2S predissociates at a relatively much faster rate, faster than the corresponding state of H_2S, which precludes the detailed study of the parent rotational level dependent fragmentation dynamics. This unusual 'inverse' isotope effect can be explained by near resonance with an excited vibrational level of a heavily predissociated, lower energy Rydberg state, that boosts the rate of nonadiabatic coupling to the dissociative continuum. However, the present high-resolution studies following excitation to the $^1B_1(4da_1 \leftarrow 2b_1)$ state at $\lambda \sim 129.1$ nm show that, as with H_2S, some D_2S molecules with $\langle J_b^2 \rangle = 0$ dissociate to D + SD(A) products. These data serve to reinforce the recent suggestion[33] that excited molecules decaying via initial coupling to the $^1A''$ continuum can further couple to the higher lying (in the vertical region) $^1A'$ PES and ultimately yield electronically excited SD(A) products along with a D atom partner. For completeness, we note that two photon excitation of D_2S (to somewhat lower total energies) has been shown to yield some rovibrationally excited D_2 products, thereby confirming – as in H_2S – the operation of one or more rival S atom elimination channels.[42]

2. EXPERIMENTAL METHODS

The product total translational energy, $P(E_T)$, distributions were determined using the D Rydberg atom time-of-flight (DRTOF) method.[43,44] The experiment has been detailed previously.[45−48] The D_2S sample (30%, in Ar carrier gas) entered the interaction volume in the form of a pulsed jet. The VUV photolysis photons (at $\lambda \sim 129.1$ or ~ 139.1 nm) were generated by difference four-wave mixing (DFWM) using two $\lambda = 212.556$ nm photons together with a third photon at, respectively, $\lambda \sim 600$ or ~ 450 nm. The various laser outputs were overlapped in time and space in a 3:1 ratio Ar/Kr gas mixture, and their wavelengths were calibrated using a wavemeter. DRTOF spectra were recorded along TOF axes at $\theta = 0°$ (parallel), 90° (perpendicular), and 54.7° (*i.e.*, magic angle) to the electric ($\boldsymbol{\varepsilon}$) vector of the incident VUV radiation, which was set using a rotatable half-waveplate positioned in the path of the ~600 or ~450 nm radiation.

DFWM methods were also used to generate VUV probe photons at the D Lyman-α wavelength, using two $\lambda = 212.556$ nm photons, a $\lambda \sim 845$ nm photon, and a 3:1 Ar/Kr gas mixture. The resulting D($n = 2$) atoms were promoted to a Rydberg state with principal quantum number, $n = 30−80$ by absorbing a further $\lambda \sim 365$ nm photon. D_2S photolysis at $\lambda = 212.556$ nm will also yield D atom photoproducts. Contributions from such unwanted photolysis to the measured DRTOF spectra were avoided in the present work by arranging that the laser beams exiting the respective Ar/Kr gas cells pass through biconvex LiF lenses that are deliberately mounted off-axis, so that only the VUV photons propagate through the interaction region.[49] The VUV probe photons also induce some D_2S photolysis, generating D atoms. This contribution was removed using a background subtraction technique, with the VUV photolysis photons present only on alternate probe laser shots.

The Rydberg-tagged D atom photofragments fly a distance $d \sim 280$ mm prior to being field ionized when they reach the grounded mesh positioned just before a microchannel plate detector. The measured TOF spectra were converted to D atom translational energy distributions and then to the corresponding $P(E_T)$ distributions using momentum conservation arguments.[43] D atom photofragment excitation (PHOFEX) spectra were obtained by integrating the D atom signal while scanning across the requisite photoexcitation wavelength range.

3. RESULTS AND DISCUSSION

3.1. Exciting the $^1B_1(4da_1 \leftarrow 2b_1)$ State of D_2S at $\lambda \sim 129.1$ nm. Figure 2A shows the D atom PHOFEX spectrum obtained when exciting a jet-cooled D_2S sample across the range of $129.16 \geq \lambda \geq 128.95$ nm (77420−77550 cm^{-1}). Each feature involves one or more lifetime broadened J_{KaKc}'-J_{KaKc}'' transitions, which can be assigned using PGOPHER[50] and relevant spectroscopic parameters. Rotational constants for the ground state neutral molecule were taken from ref 51, while parameters for the ground state D_2S^+ ion[52] were assumed for the Rydberg state. The resulting simulation, both in the form

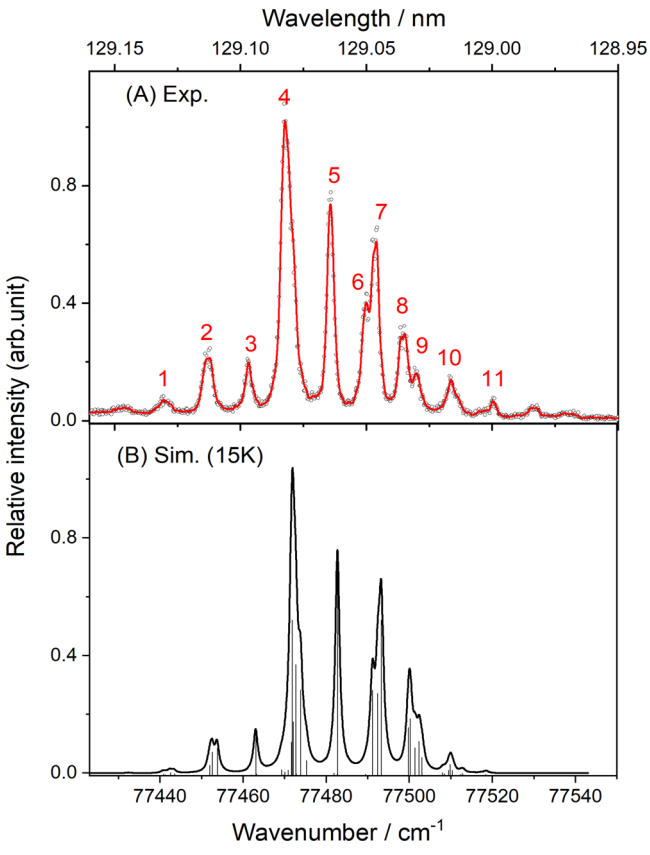

Figure 2. (A) D atom PHOFEX spectrum recorded over the range $129.16 \geq \lambda \geq 128.95$ nm using a jet-cooled 30% D_2S in Ar gas mixture. (B) PGOPHER simulation of this $D_2S(^1B_1$-$\tilde{X}^1A_1)$ band using spectroscopic parameters from refs 51, 52, a band origin $\nu_0 = 77473$ cm^{-1} and rotational and nuclear spin temperatures $T_{rot} = 15$ K and $T_{ns} = 300$ K, respectively. The simulated spectrum is shown both in stick form and with each rovibronic transition clothed with a 1.3 cm^{-1} full width half-maximum (fwhm) Lorentzian line shape.

https://doi.org/10.1021/acs.jpca.4c04730
J. Phys. Chem. A XXXX, XXX, XXX−XXX

of a stick spectrum and with a line width assigned to each transition, is shown in Figure 2B. This allowed identification of the dominant contributions to the measured peaks (labeled 1−11 in Figure 2A) and determination of the $^1B_1$-$\tilde{X}^1A_1$ band origin (ν_0 = 77473 cm^{-1}). The simulation identifies features 3 and 5 at λ = 129.097 nm (77461.1 cm^{-1}) and 129.064 nm (77480.9 cm^{-1}) as essentially pure single rovibronic transitions (the 0_{00}-1_{10} and 1_{10}-0_{00} lines, respectively), and suggests that peaks 7 and 8 at 129.046 and 129.035 nm (77491.7 and 77498.4 cm^{-1}) are dominated by, respectively, the 2_{21}-1_{11} transition and the blended 3_{12}-2_{02} and 3_{21}-2_{11} transitions. Table 2 reports these and some of the stronger transitions that

Table 2. Wavelengths/Wavenumbers of Maxima in the D Atom PHOFEX Spectrum Measured at $\lambda \sim$ 129.1 nm (Figure 2A) and Dominant Contributing Transitions Identified by the PGOPHER Simulation (Figure 2B)[a]

peak	measured wavelength/nm	wavenumber/ cm^{-1}	transition	$\langle J_b^2 \rangle$
1	129.130	77441.3	**2_{12}-3_{22}**	**1.00**
2	129.113	77451.5	**1_{10}-2_{20}, 1_{01}-2_{11}**	**1.00, 1.00**
3	129.097	77461.1	0_{00}-1_{10}	0
4	129.082	77470.1	**1_{01}-1_{11}, 2_{12}-2_{02}**	**1.00, 1.00**
5	129.064	77480.9	**1_{10}-0_{00}**	**1.00**
6	129.050	77489.3	2_{11}-1_{01}	4.00
7	129.046	77491.7	**2_{21}-1_{11}**	**1.00**
8	129.035	77498.4	**3_{12}-2_{02}, 3_{21}-2_{11}**	**6.13, 8.13**
9	129.029	77502.0	**3_{30}-2_{20}**	**3.87**
10	129.016	77509.8	**4_{23}-3_{13}, 4_{32}-3_{22}**	**6.47, 7.62**
11	129.000	77519.4	**5_{14}-4_{04}**	**8.60**

[a]Transitions of *ortho*-D_2S molecules are highlighted in bold, and the final column shows $\langle J_b^2 \rangle$, the expectation value of the square of the angular momentum about the *b*-inertial axis for the various excited rotational levels.

contribute to the other more heavily blended features 1−11, together with the $\langle J_b^2 \rangle$ values (the expectation values of the square of the angular momentum about the *b*-inertial axis) in the respective J_{KaKc}' levels.

Several factors influence the relative intensities of the various features in this D atom PHOFEX spectrum. The two identical D atoms ensure that each D_2S rotational level obeys either the *ortho*- or *para*-nuclear spin statistics. The *ortho*- levels (identifiable as those with $K_a + K_c$ = even in the $\tilde{X}$ state) have a 2-fold higher statistical weight. Transitions of *ortho*-D_2S molecules are identified in bold in Table 2. The *ortho*- and *para*-D_2S molecules do not interconvert during the supersonic expansion, and the simulation shown in Figure 2B assumes rotational and nuclear spin temperatures of, respectively, T_{rot} = 15 K and T_{ns} = 300 K. The measured PHOFEX spectrum is necessarily a convolution of the parent absorbance and the branching ratio for fragmentation to yield one (or two) D atoms. Analogy with the H_2S suggests that the D_2 elimination channels have small quantum yields at the wavelengths of current interest.[32] Thus the D atom PHOFEX spectrum is best compared to the parent absorption spectrum predicted by PGOPHER (Figure 2B). As in our earlier considerations of the corresponding $^1B_1(nda_1 \leftarrow 2b_1; n = 3, 4)$ transitions in H_2S,[32,33] however, it is necessary to recognize some further subtleties.

First, the intensity of the signal between the peaks in Figure 2A is not zero. This is unsurprising, given the background continuum in the parent absorption spectrum (Figure 1), but PGOPHER by design simulates only the $^1B_1$-$\tilde{X}^1A_1$ transition probability. The nonzero D atom signal across the wavelength range spanned in Figure 2A implies some probability for direct excitation to the underlying continuum and dissociation to D + SD products. However, the peaks in the PHOFEX spectrum show no obvious asymmetry, such as that might be expected as a result of Fano interference between the excitation pathways to the Rydberg levels and to the continuum. This likely reflects the comparative weakness of the continuum absorption. Second, the J_{KaKc}' levels in the $^1B_1(nda_1 \leftarrow 2b_1; n = 3,4)$ states of H_2S predissociate by rival rotational level dependent and rotational level independent pathways. The rate of the former (Coriolis-driven) pathway scales with $\langle J_b^2 \rangle$.[32,33] Coriolis-driven nonadiabatic coupling contributes to the decay of D_2S molecules in the $^1B_1(4da_1 \leftarrow 2b_1)$ state also (see later), but its relative contribution to the overall loss rate is less apparent than in the H_2S cases. The simulation shown in Figure 2B, with no explicit inclusion of $\langle J_b^2 \rangle$-specific line broadening effects, suffices to allow unambiguous assignment of all contributing features. Third, the present $P(E_T)$ spectra (see below) show substantial yields of the SD(A) radical products. All SD(A) fragments apart from those formed in the $v' = 0$ level with low N' rotational quantum number will predissociate within the ∼10 ns delay between the pump and probe excitations.[34,36] Dissociations yielding such D + SD(A) primary products will thus yield a net two D atoms per absorbed photolysis photon, and peaks in the D atom PHOFEX spectrum associated with transitions to J_{KaKc}' levels that favor formation of internally excited SD(A) products should thus be expected to appear with greater relative intensity than predicted by the PGOPHER simulation.

Figure 3 shows D atom TOF spectra measured following excitation to the J_{KaKc}' = (a) 0_{00}, (b) 1_{10}, and the (c) $3_{12}/3_{21}$ levels (*i.e.* excitation of peaks 3, 5, and 8 in Figure 2A) with the polarization ($\boldsymbol{\varepsilon}$) vector of the photolysis radiation aligned both parallel ($\theta = 0°$) and perpendicular ($\theta = 90°$) to the detection axis. These transitions access excited state levels with $\langle J_b^2 \rangle$ = 0, 1, and ∼7, respectively. Equivalent data obtained when exciting most of the other features labeled in Figure 2A are shown in Figure S1 in the Supporting Information (SM) where, again, the spectra have been ordered in terms of increasing $\langle J_b^2 \rangle$ for the excited state levels populated via the stronger contributing transitions identified in Table 2. Both sets of spectra show that the relative intensity of the early part of the TOF spectrum (the high E_T component) decreases on moving down the figure (*i.e.*, when accessing levels with higher $\langle J_b^2 \rangle$). Figure 3b also demonstrates that the high and low E_T products show very different recoil anisotropies, particularly when exciting to the 1_{10} level via line 5 (panel B). Similarly striking product state-dependent recoil anisotropies have been noted previously when exciting the 1_{10}-0_{00} line in the origin bands of the $\tilde{C}^1B_1$-$\tilde{X}^1A_1$ transition of H_2O[53,54] and of the $^1B_1$-$\tilde{X}^1A_1$ transition of H_2S at $\lambda \sim$ 139.1 nm.[32]

The D atom TOF data were converted to the corresponding total (D + SD) translational energy distributions, $P(E_T)$, using eq 1

$$E_T = \frac{1}{2} m_D \left(\frac{d}{t}\right)^2 \left(1 + m_D/m_{SD}\right) \quad (1)$$

https://doi.org/10.1021/acs.jpca.4c04730
J. Phys. Chem. A XXXX, XXX, XXX−XXX

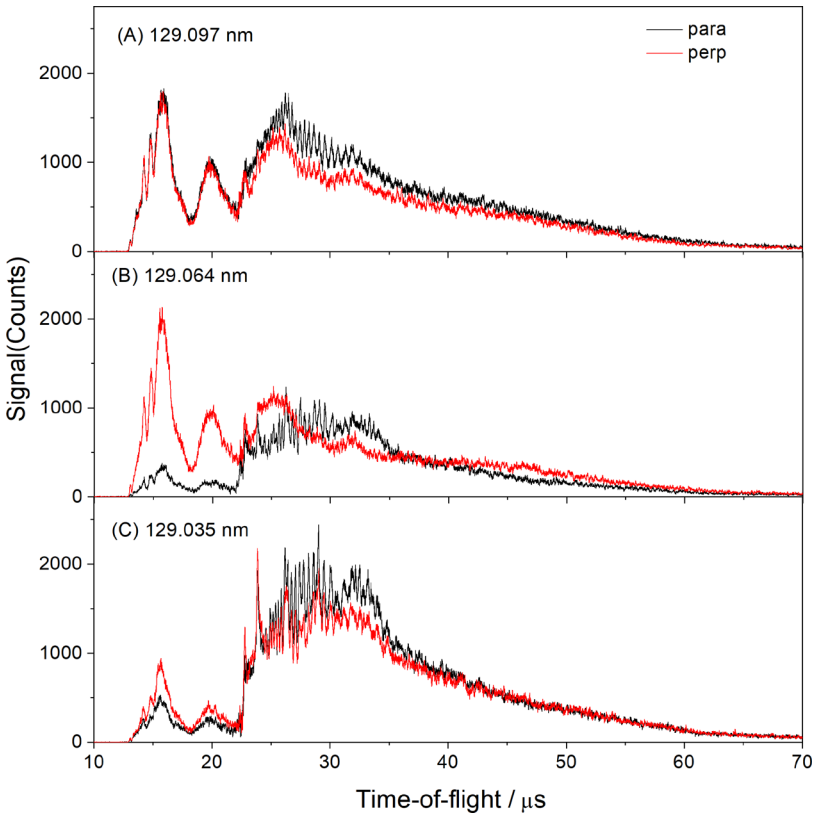

Figure 3. D atom TOF spectra obtained following photolysis of a jet-cooled 30% D_2S in Ar sample at (A) 129.097 nm, (B) 129.064 nm, and (C) 129.035 nm (*i.e.*, exciting on peaks 3, 5 and 8 in Figure 2A), sampling predominantly or exclusively the 0_{00}, 1_{10} and $3_{12}/3_{21}$ excited state levels. Data measured with the $\boldsymbol{\varepsilon}$ vector of the photolysis laser radiation aligned parallel ($\theta = 0°$) and perpendicular ($\theta = 90°$) to the detection axis are shown in black and red, respectively.

Here, m_D and m_{SD} are the respective masses of the D atom and SD radical fragments, d is the distance separating the interaction region and the detector, and t is the D atom TOF measured over this distance. Figure 4 shows $P(E_T)$ spectra obtained at the wavelengths featured in Figure 3, again with $\boldsymbol{\varepsilon}$ aligned both parallel and perpendicular to the detection axis. The corresponding $P(E_T)$ spectra derived from the D atom TOF spectra displayed in Figure S1 are shown in Figure S2 in the SM. The vertical arrows in the main panel show the maximum E_T values associated with D atom formation via channels I–IV, while the combs in panels (A) and (B) show the E_T values associated with forming D atoms together with SD(X) fragments in selected v'', N'' levels. The inset in panel C shows an expanded view of the lower E_T region, with the combs indicating the E_T values associated with formation of D plus SD(A) fragments in selected v', N' levels.

The density of SD(X) and SD(A) rovibrational levels populated in all cases prevents unique characterization of the product quantum state population distributions, but the superposed combs clearly show that excitation on all features in the D atom PHOFEX spectrum results in SD(X) products in a wide range of rovibrational quantum states, some with minimal internal energy, E_{int}, and others with E_{int} values approaching the upper limit supported by the SD(X) potential. The E_T region associated with D + SD(A) products is shown on an expanded scale in the inset in panel (C); the superposed combs suggest that the SD(A) products are preferentially formed in the $v' = 0$ level, in a very wide range of N' levels.

Figure 5A–C shows $P(E_T)$ spectra taken with $\boldsymbol{\varepsilon}$ aligned at $\theta = 54.7°$ (*i.e.*, at the magic angle) to the detection axis following excitation on lines 3, 5, and 8 in the D atom PHOFEX spectrum, and equivalent spectra obtained from the sum $(I(0°) + 2I(90°))/3$, where $I(0°)$ and $I(90°)$ are the corresponding spectral profiles measured under equivalent conditions but with $\boldsymbol{\varepsilon}$ aligned at $\theta = 0$ and 90° (*i.e.*, the spectra shown in Figure 4). The magic-angle spectra derived via these alternative methods are reassuringly similar. Analyses of such $P(E_T)$ spectra offer a route to estimating the branching between primary product channels I and II. In each case, the $P(E_T)$ spectrum was split at the E_T value of the onset for channel II, $E_T(2)$, and the integrated intensity of signal with $E_T > E_T(2)$ was taken as a measure of the D + SD(X) yield. Signal with $E_T < E_T(2)$ can derive from channel II, from the rapid predissociation of most primary SD(A) fragments, and from channels III and IV. The $P(E_T)$ spectra suggest that the three body fragmentation channels are both rather minor contributors at these excitation wavelengths. Thus the primary yield of channel II products is approximated as half the total signal measured with $E_T < E_T(2)$. Figure 5D shows the estimated primary SD(A)/SD(X) yield climbing with increasing $\langle J_b^2 \rangle$, as expected given that b-axis rotation has the appropriate symmetry to enable Coriolis coupling to the $^1A'$ continuum that correlates with D + SD(A) products. However, Figure 5D also shows that this ratio is far from zero when exciting to levels with $\langle J_b^2 \rangle = 0$. Similar trends were noted when exciting to different parent levels within the corresponding $^1B_1$-$\tilde{X}^1A_1$ transition of H_2S,[33] though as Figure 5D also shows, the SH(A)/SH(X) ratio when exciting H_2S levels with $\langle J_b^2 \rangle = 0$ was much lower and the ratio increased with increasing $\langle J_b^2 \rangle$ at

https://doi.org/10.1021/acs.jpca.4c04730
J. Phys. Chem. A XXXX, XXX, XXX–XXX

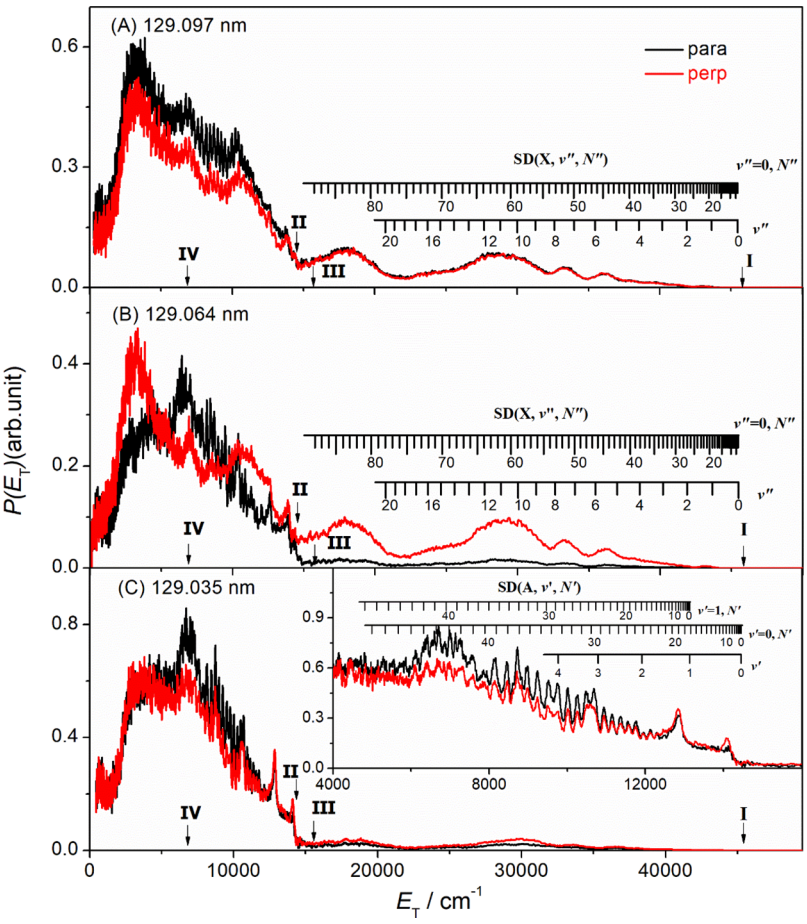

Figure 4. $P(E_T)$ spectra derived from D atom TOF spectra obtained following photodissociation of D_2S at (A) 129.097 nm, (B) 129.064 nm, and (C) 129.035 nm with $\boldsymbol{\varepsilon}$ aligned, respectively, parallel ($\theta = 0°$, black) and perpendicular ($\theta = 90°$, red) to the detection axis. The vertical arrows in each panel show the maximum E_T values associated with D atom formation via channels I–IV. The combs in (A) and (B) show the E_T values associated with formation of D plus SD(X) fragments in selected v'', N'' levels, while the inset in (C) shows an expanded view of the lower E_T region, with the superposed combs defining the E_T values associated with formation of D plus SD(A) fragments in selected v', N' levels.

a steeper rate (consistent with the larger B rotational constant in the lighter isotopomer).

These data broadly accord with the 'big picture' description developed previously.[31] D_2S molecules in the $^1B_1(4da_1 \leftarrow 2b_1)$ Rydberg state can predissociate homogeneously, by coupling to the valence continuum of $^1A''$ symmetry, and heterogeneously, by Coriolis coupling to the $^1A'$ continuum, with relative efficiencies that depend on the rotational angular momentum of the particular J_{KaKc}' level. Both continua are recognized as involving more than one coupled state, and recent electronic structure calculations have confirmed regions of degeneracy between the respective PESs (conical intersections between surfaces of the same symmetry, and seams of intersection between $^1A''$ and $^1A'$ surfaces at linear geometries).[31] Molecules that couple to and remain in the $^1A''$ states dissociate to D + SD(X) products (channel I) or, at sufficiently short excitation wavelengths, conceivably to 2D + $S(^3P)$ products (channel III). The topographies of the $^1A''$ state PES(s) encourage formation of SD(X) products in a wide spread of v'', N'' levels.

The nonadiabatic coupling of D_2S molecules in Rydberg states with $^1B_1$ symmetry to the $^1A'$ PES(s) is enabled by b-axis rotation. Molecules on the $^1A'$ PES(s) can experience a variety of possible fates.[31] Of most relevance to the present study, those that avoid the linear geometries required for further nonadiabatic coupling (to the $^1A''$ PES(s)) remain on the $^1A'$ PES(s) and can dissociate to D + SD(A) products. The topography of the lowest $^1A'$ PES encourages opening of the ∠DSD bond angle in tandem with D···SD bond extension, and this motion carries through into rotational excitation of the SD(A) products. As with H_2S,[31] the lower D + SD(X) yields (*i.e.* high SD(A)/SD(X) product ratios) from D_2S molecules prepared with higher $\langle J_b^2 \rangle$ imply that, after coupling to the $^1A'$ PES(s), the probability of further coupling to the $^1A''$ PES(s) is low. The relative strengths of the D···SD stretching and ∠DSD angle opening forces on the $^1A'$ PES ensure that the dissociating molecules attain linear configurations at D···SD extensions beyond the range that supports nonadiabatic coupling to the $^1A''$ PES(s).

The present data reinforce another finding from recent photolysis studies of H_2S following excitation to the analogous Rydberg state. Excitation at $\lambda = 129.097$ nm (peak 3 in Figure 2A) populates the 0_{00} level of this $^1B_1$ state, which nonetheless gives a substantial D + SD(A) product yield (Figure 4A). The SD(A)/SD(X) ratio is ∼ 1.7. The SD(A) product from the rotationless level implies the operation of an additional fragmentation mechanism. As before, population decay from this rotationless level must start with vibronic coupling to the $^1A''$ continuum. As noted above, the $^1A''$ and $^1A'$ PES(s) are nearly degenerate over a range of near-linear geometries. The

https://doi.org/10.1021/acs.jpca.4c04730
J. Phys. Chem. A XXXX, XXX, XXX−XXX

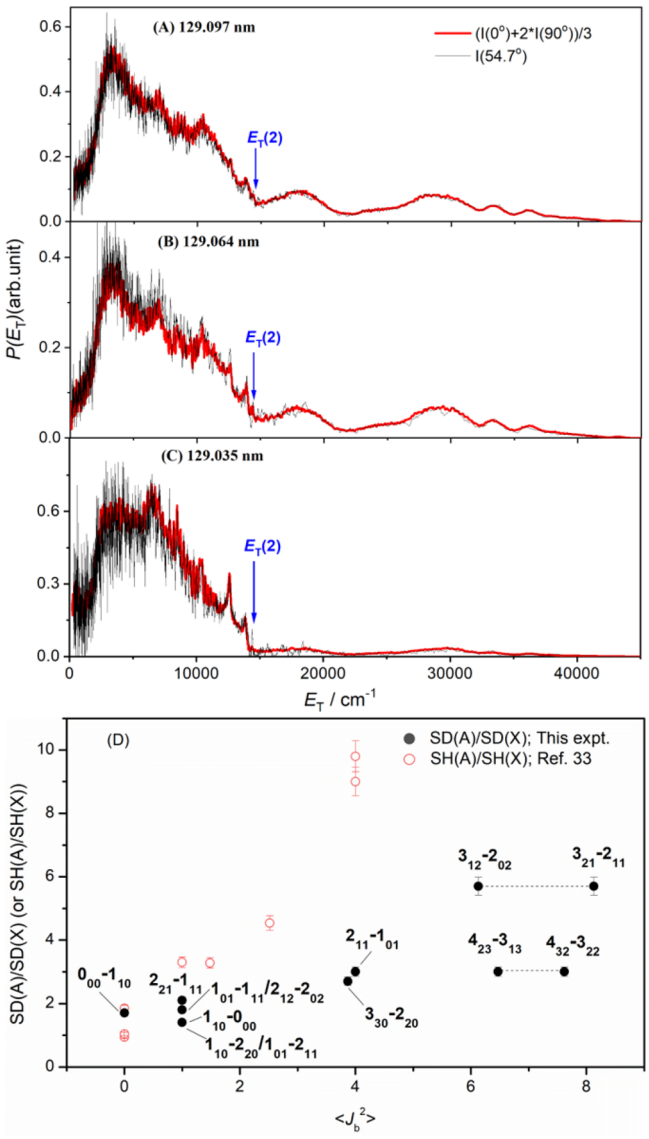

Figure 5. $P(E_T)$ spectra obtained following photodissociation of D_2S at (A) 129.097 nm, (B) 129.064 nm, and (C) 129.035 nm, with $\boldsymbol{\varepsilon}$ aligned at $\theta = 54.7°$ to the detection axis (black lines), and equivalent spectra obtained from the sum $(I(0°) + 2I(90°))/3$, where $I(0°)$ and $I(90°)$ are the corresponding spectral profiles measured under equivalent conditions but with $\boldsymbol{\varepsilon}$ aligned at $\theta = 0$ and 90°. (D) Primary SD(A)/SD(X) product ratio (black points), obtained by comparing the total signal with $E_T > E_T(2)$ with half the total signal with $E_T < E_T(2)$, plotted as a function of $\langle J_b^2 \rangle$ for the parent excited level(s) excited with greatest probability at nine different wavelengths within the $^1B_1$-$\tilde{X}^1A_1$ band at $\lambda \sim 129.1$ nm. The corresponding plot of SH(A)/SH(X) vs $\langle J_b^2 \rangle$ determined when exciting the equivalent band of H_2S (from ref 33) is included for comparison (pink open symbols).

nonadiabatic coupling in these regions has usually been discussed as a means of passing population from the $^1A'$ PES(s) to the lower energy (viewed in terms of their respective energies in the vertical Franck–Condon region) $^1A''$ PES(s). However, the photoprepared molecules here access the $^1A''$ PES(s) at high total energy (~9.6 eV relative to the ground state minimum energy geometry), and the topography of the $^1A''$ PES(s) is assumed to allow some of these molecules to sample regions of near-degeneracy with the $^1A'$ PES, and couple to the $^1A'$ PES with nuclear momenta appropriate to access the D + SD(A) limit. Within the traditional framework of radiationless transition theory, such coupling of internally excited molecules into a high-energy electronic state might be viewed as an 'uphill' internal conversion.

3.2. Photoexciting the $^1B_1(3da_1 \leftarrow 2b_1)$ State of D_2S at $\lambda \sim 139.1$ nm. Figure 6 shows the D atom PHOFEX spectrum obtained following excitation of this $^1B_1$-$\tilde{X}^1A_1$ band of D_2S together with a PGOPHER[50] simulation that, again, employs documented spectroscopic parameters for the ground state[51] and assumes that the rotational constants for the Rydberg state are well approximated by those of the ground state molecular ion.[52] In contrast to the corresponding feature in the H_2S spectrum,[33] the measured D_2S resonance is much broader than predicted by the PGOPHER simulation. The more intense region centered at $\lambda \sim 139.05$ nm shows an obvious band contour, but no resolved rotational fine structure. There is no unique fit for such a relatively featureless contour. Individual rovibronic linewidths in the displayed simulation are modeled as the sum of homogeneous and heterogeneous contributions, using the function $\omega = \omega_0 + \omega' \langle J_b^2 \rangle$, with $\omega_0 =$

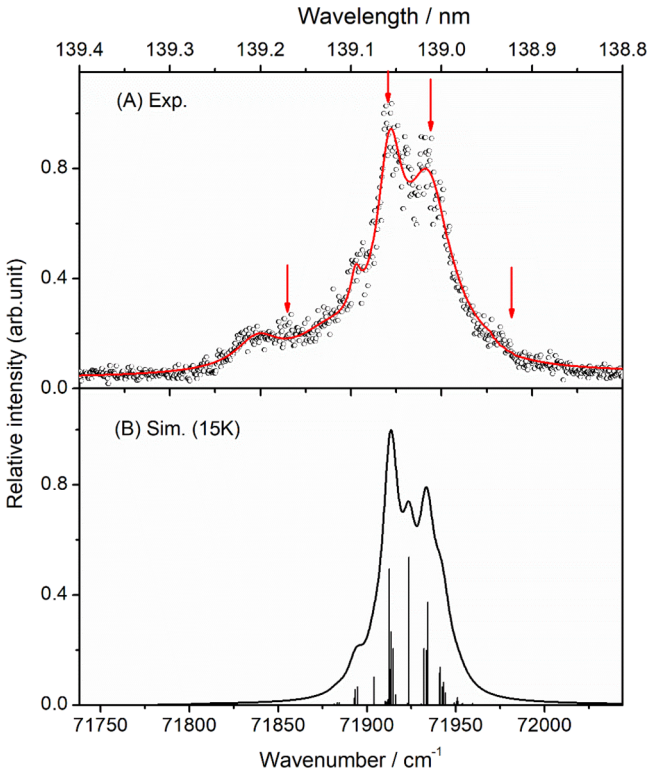

Figure 6. (A) D atom PHOFEX spectrum recorded over the range $139.4 \geq \lambda \geq 138.8$ nm using a jet cooled 30% D_2S in Ar gas mixture. The vertical arrows indicate the four wavelengths at which D atom TOF spectra were recorded. (B) PGOPHER simulation of this $D_2S(^1B_1$-$\tilde{X}^1A_1)$ band using spectroscopic parameters from refs 51, 52, and a band origin $\nu_0 = 71914$ cm^{-1}. The simulated spectrum is shown both in stick form and with each rovibronic transition clothed with a Lorentzian line shape with a fwhm determined by the excited state lifetime. The transition widths are modeled as the sum of homogeneous and heterogeneous contributions, using the function $\omega = \omega_0 + \omega' \langle J_b^2 \rangle$ with $\omega_0 = 10$ cm^{-1} and $\omega' = 0.15$ cm^{-1} (though the quality of the match with experiment was rather insensitive to the choice of ω' value), and the peak amplitudes have been reduced in a compensatory manner to conserve the calculated rovibronic transition linestrength. The simulation assumes rotational and nuclear spin temperatures $T_{rot} = 15$ K and $T_{ns} = 300$ K, respectively.

https://doi.org/10.1021/acs.jpca.4c04730
J. Phys. Chem. A XXXX, XXX, XXX−XXX

10 cm^{-1} and $\omega' = 0.15$ cm^{-1}. Increasing ω' to 2 cm^{-1} causes little change to the band contour, but any significant reduction in the ω_0 value (which is much larger than for the corresponding band of H_2S) leads to the emergence of some sharper features within the overall contour—in contrast to the experimental observation.

Such an 'inverse' isotope effect (*i.e.*, where the state of a deuteride predissociates faster than the same state in the corresponding hydride) is unusual, but not without precedent. Indeed, the present example has been noted in previous room temperature absorption studies of the $^1B_1(3da_1 \leftarrow 2b_1)$ states of D_2S and H_2S when exciting at $\lambda \sim 139.1$ nm,[55] and rationalized by invoking accidental near-resonance with a vibrationally excited level of some lower lying Rydberg state. Mayhew[56] noted the likely near degeneracy of the $^1B_1(3da_1 \leftarrow 2b_1)$ state of D_2S with the first excited bending vibrational level (the 010 level) of the more heavily predissociated $^1B_2(3da_2 \leftarrow 2b_1)$ state and suggested this as a plausible doorway state promoting access to the dissociative continua. Given the mass (and frequency) differences upon substituting H for D, there is no corresponding accidental degeneracy between the $^1B_1(3da_1 \leftarrow 2b_1$, 000) and $^1B_2(3da_2 \leftarrow 2b_1$, 010) levels in H_2S. Though appealing, we conclude that this is unlikely to be the dominant interaction that enhances predissociation of the $^1B_1(3da_1 \leftarrow 2b_1$, 000) state of D_2S. The two states have different vibronic symmetries and would require an a_2 coupling mode (*e.g.*, rotation about the *c*-axis (the out-of-plane axis) in D_2S). The unambiguous conclusion from the PGOPHER simulations, however, is that the enhanced predissociation rate is mostly homogeneous in nature. Thus, though retaining the accidental resonance model, it seems much more likely that the doorway state facilitating predissociation of the $^1B_1(3da_1 \leftarrow 2b_1)$ state of D_2S at $\lambda \sim 139.1$ nm is the (100) level of the other (lower lying) $^1B_1(3da_1 \leftarrow 2b_1)$ state of D_2S, the first member of Price's C series.[22] The symmetric stretch vibration in D_2S has a wavenumber $\nu_1 \sim 1896$ cm^{-1} [ref 57], some 750 cm^{-1} smaller than in H_2S, so there will be no equivalent near-resonant doorway from the $^1B_1(3da_1 \leftarrow 2b_1)$ origin level to the background continua in H_2S. A similar accidental resonance enhanced, albeit 'regular', isotope effect has been reported for the respective (010) levels of the $\tilde{C}^1B_1$ state of H_2O and D_2O. Accidental degeneracy with the origin level of the more heavily dissociated $\tilde{D}^1A_1$ state ensures that the $\tilde{C}(010)$ level of H_2O predissociates much faster than (and displays different fragmentation dynamics to) its counterpart in D_2O.[58]

D atom TOF spectra following D_2S photolysis were taken at the four excitation wavelengths indicated by vertical arrows in Figure 6, again with $\boldsymbol{\varepsilon}$ aligned at $\theta = 0°$ (black) and 90° (red) from the detection axis. These are displayed in Figure 7 and the corresponding $P(E_T)$ spectra are shown in Figure 8. The two spectra taken at wavelengths within the more intense region spanned by the predicted $^1B_1$-$\tilde{X}^1A_1$ band contour are very similar, consistent with dissociation from a broad mix of excited levels in each case. The spectra show SD(X) and SD(A) fragment formation in a wide range of rovibrational levels, with clear evidence for the population of SD(A, low v', high N') levels. The SD(A)/SD(X) ratio estimated as above from the ratio of half the total yield with $E_T < E_T(2)$ relative to the total yield with $E_T > E_T(2)$ is ~ 0.44. In both cases, dissociation shows a mild preference for a perpendicular recoil.

The $P(E_T)$ spectra obtained at the two other wavelengths, off-resonant with the predicted $^1B_1$-$\tilde{X}^1A_1$ band, show higher SD(A)/SD(X) ratios (particularly at $\lambda \sim 139.170$ nm, where the ratio is ~ 0.75) and more dramatic, product state-dependent, recoil anisotropies. Peaks attributable to SD(A, v'=0, and high N') products are very obvious at both excitation wavelengths. Most display preferential perpendicular recoil anisotropy, but SD(A, v'=0) products in the very highest N' levels (and SD(A, v'=1, high N')) show more strongly at θ = 0°. The expanded views of the $P(E_T)$ distributions shown in the insets in panels (A) and (D) also show an obvious tail declining toward the E_T value associated with threshold III, which is most logically attributed to D atoms from the predissociation of primary SD(A, high N') products.

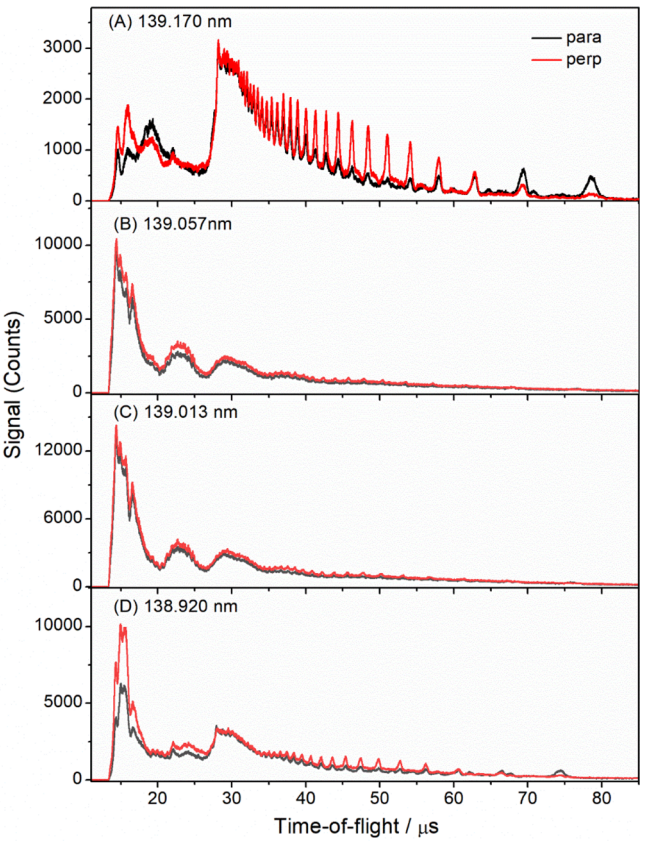

Figure 7. D atom TOF spectra obtained following photolysis of a jet-cooled 30% D_2S in Ar sample at (A) 139.170 nm, (B) 139.057 nm, (C) 139.013 nm, and (D) 138.920 nm (shown by the vertical arrows in the D atom PHOFEX spectrum (Figure 6A) measured with the $\boldsymbol{\varepsilon}$ vector of the photolysis laser radiation aligned parallel ($\theta = 0°$, black) and perpendicular ($\theta = 90°$, red) to the detection axis.

4. CONCLUSIONS

This article reports high-resolution translational spectroscopy studies of the D atoms formed from two predissociated Rydberg states of D_2S following excitation at $\lambda \sim 139.1$ and ~ 129.1 nm. Both states have $^1B_1$ symmetry and the photofragmentation dynamics of the corresponding excited states of H_2S have been investigated recently.[32,33] In both cases, D−SD (H−SH) bond fission is deduced to be the dominant dissociation pathway, yielding SD(SH) fragments in both the ground ($X^2\Pi$) and excited ($A^2\Sigma^+$) electronic states. The X state products are distributed over a very broad range of v'', N'' levels, while the A state products are mostly formed in levels with low v' and high N'. Such energy partitioning in the products is explicable (at least qualitatively) by reference to the topographies of the PES(s) of the $^1A''$ and $^1A'$ continuum

https://doi.org/10.1021/acs.jpca.4c04730
J. Phys. Chem. A XXXX, XXX, XXX−XXX

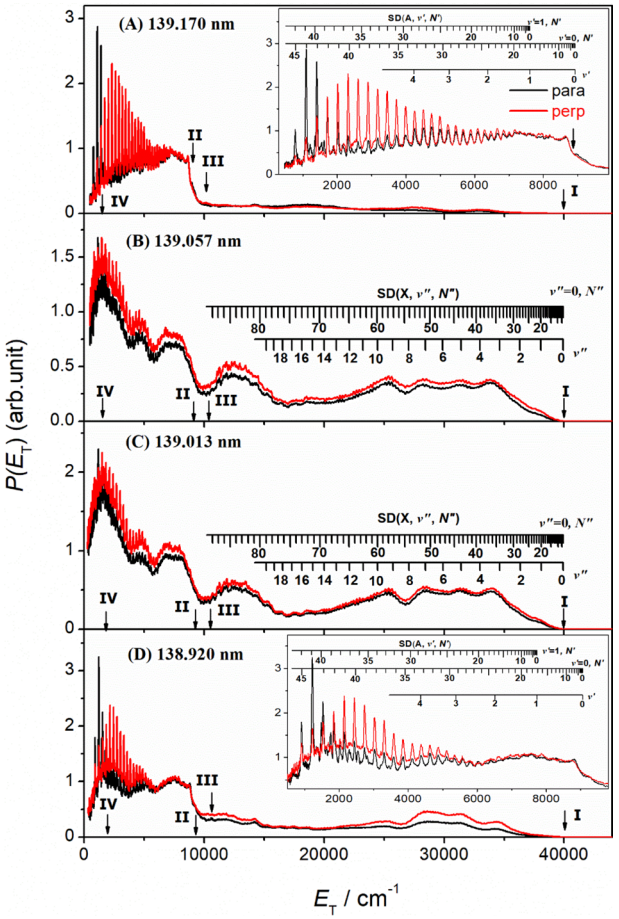

Figure 8. $P(E_T)$ spectra derived from the D atom TOF spectra obtained following photodissociation of D_2S at (A) 139.170 nm, (B) 139.057 nm, (C) 139.013 nm, and (D) 138.920 nm with $\boldsymbol{\varepsilon}$ aligned, respectively, parallel (θ = 0°, black) and perpendicular (θ = 90°, red) to the detection axis. The vertical arrows in all four panels show the maximum E_T values associated with D atom formation via channels I-IV. The combs in (B) and (C) show the E_T values associated with formation of D plus SD(X) fragments in selected v'', N'' levels. The insets in panels (A) and (D) show expanded views of the lower E_T region, with the superposed combs defining the E_T values associated with formation of D plus SD(A) fragments in selected v', N' levels.

states that support the respective dissociation pathways. H/D isotopic substitution has strikingly different effects on the fragmentation dynamics of these two $^1B_1$ states.

In the case of the $^1B_1(4da_1 \leftarrow 2b_1)$ state of D_2S populated by excitation at $\lambda \sim 129.1$ nm, the D atom PHOFEX spectrum shows resolved rotational fine structure, which has allowed investigation of how the rotational angular momentum of the excited state parent molecule influences the fragmentation dynamics. As in H_2S, the *b*-axis rotational motion is found to boost the relative yield of D + SD(A) products, implying the operation of a Coriolis-induced dissociation pathway via coupling to the $^1A'$ continuum. However, SD(A) products are still a major dissociation product for D_2S molecules excited to the 0_{00} rotational level, for which $\langle J_b^2 \rangle = 0$. The SD(A)/SD(X) product ratio in this case is still ~ 1.7. This finding confirms the operation of an additional fragmentation mechanism, adding weight to a recent proposal that the dissociation of excited levels of D_2S (H_2S) can also occur by initial vibronic coupling to the $^1A''$ continuum, with subsequent nonadiabatic coupling to the $^1A'$ PES allowing access to the D + SD(A) limit.[33] In the framework of traditional radiationless transition theory, the transfer of internally excited molecules into a higher energy electronic state en route to dissociation could be viewed as an 'uphill' internal conversion.

The D atom PHOFEX spectrum when exciting the $^1B_1(3da_1 \leftarrow 2b_1)$ state of D_2S at $\lambda \sim 139.1$ nm, in contrast, is devoid of rotational fine structure. The corresponding band in the spectrum of H_2S is structured.[22−24,27,28,32] This finding is noteworthy, but not without precedent. Predissociation rates are (as here) typically determined by a nuclear kinetic energy operator and will typically be larger for the lighter species (*i.e.*, H_2S). The $^1B_1(3da_1 \leftarrow 2b_1)$ state of $D_2S(H_2S)$ shows an 'inverse' isotope effect; the heavier isotopomer predissociates faster. This finding is rationalized by recognizing the role of an accidentally resonant 'doorway' state, the (100) level of the other (lower lying and more heavily predissociated) $^1B_1(3da_1 \leftarrow 2b_1)$ state of D_2S, that facilitates coupling to the $^1A''$ continuum. The normal modes of vibration in the different isotopomers have different energies, and no such accidental resonance is available to assist the predissociation of the corresponding state of H_2S populated when exciting at $\lambda \sim 139.1$ nm. The uncertainty broadening caused by the short excited-state lifetime precluded the study of parent-level dependent fragmentation dynamics or product state distributions in this case. Nonetheless, D_2S excitation at $\lambda \sim 139.1$ nm clearly yields SD(A) and SD(X) products, in both cases populating similar families of rovibrational levels as when exciting at $\lambda \sim 129.1$ nm. The SD(A)/SD(X) ratios are lower, however, consistent with the 'doorway' state promoting coupling to the $^1A''$ continuum (which correlates with D + SD(X) products).

■ ASSOCIATED CONTENT

Supporting Information

The Supporting Information is available free of charge at https://pubs.acs.org/doi/10.1021/acs.jpca.4c04730.

D atom TOF spectra recorded when exciting on peaks 2, 4, 7, 6, 9, and 10 in the D atom PHOFEX spectrum recorded at $\lambda \sim 129.1$ nm (shown in Figure 2) with $\boldsymbol{\varepsilon}$ aligned, respectively, parallel and perpendicular to the detection axis, along with the corresponding $P(E_T)$ spectra derived for θ = 0° and 90° (PDF)

■ AUTHOR INFORMATION

Corresponding Authors

Michael N.R. Ashfold − *School of Chemistry, University of Bristol, Bristol BS8 1TS, U.K.;* orcid.org/0000-0001-5762-7048; Email: mike.ashfold@bristol.ac.uk

Kaijun Yuan − *State Key Laboratory of Molecular Reaction Dynamics and Dalian Coherent Light Source, Dalian Institute of Chemical Physics, Chinese Academy of Sciences, Dalian 116023, China; University of Chinese Academy of Sciences, Beijing 100049, China; Hefei National Laboratory, Hefei 230088, China;* orcid.org/0000-0002-5108-8984; Email: kjyuan@dicp.ac.cn

Authors

Zijie Luo − *Marine Engineering College, Dalian Maritime University, Dalian, Liaoning 116026, China; State Key Laboratory of Molecular Reaction Dynamics and Dalian*

https://doi.org/10.1021/acs.jpca.4c04730
J. Phys. Chem. A XXXX, XXX, XXX−XXX

Coherent Light Source, Dalian Institute of Chemical Physics, Chinese Academy of Sciences, Dalian 116023, China

Shuaikang Yang − *State Key Laboratory of Molecular Reaction Dynamics and Dalian Coherent Light Source, Dalian Institute of Chemical Physics, Chinese Academy of Sciences, Dalian 116023, China; Department of Chemical Physics, School of Chemistry and Materials Science, University of Science and Technology of China, Hefei, Anhui 230026, China*

Yucheng Wu − *State Key Laboratory of Molecular Reaction Dynamics and Dalian Coherent Light Source, Dalian Institute of Chemical Physics, Chinese Academy of Sciences, Dalian 116023, China; University of Chinese Academy of Sciences, Beijing 100049, China*

Zhenxing Li − *State Key Laboratory of Molecular Reaction Dynamics and Dalian Coherent Light Source, Dalian Institute of Chemical Physics, Chinese Academy of Sciences, Dalian 116023, China*

Wei Hua − *State Key Laboratory of Molecular Reaction Dynamics and Dalian Coherent Light Source, Dalian Institute of Chemical Physics, Chinese Academy of Sciences, Dalian 116023, China*

Zhichao Chen − *State Key Laboratory of Molecular Reaction Dynamics and Dalian Coherent Light Source, Dalian Institute of Chemical Physics, Chinese Academy of Sciences, Dalian 116023, China*

Li Che − *Department of Physics, School of Science, Dalian Maritime University, Dalian 116026, China*

Xingan Wang − *Department of Chemical Physics, School of Chemistry and Materials Science, University of Science and Technology of China, Hefei, Anhui 230026, China;* orcid.org/0000-0002-1206-7021

Xueming Yang − *State Key Laboratory of Molecular Reaction Dynamics and Dalian Coherent Light Source, Dalian Institute of Chemical Physics, Chinese Academy of Sciences, Dalian 116023, China; Hefei National Laboratory, Hefei 230088, China; Department of Chemistry and Center for Advanced Light Source Research, College of Science, Southern University of Science and Technology, Shenzhen 518055, China;* orcid.org/0000-0001-6684-9187

Complete contact information is available at: https://pubs.acs.org/10.1021/acs.jpca.4c04730

Notes

The authors declare no competing financial interest.

■ ACKNOWLEDGMENTS

M.N.R.A. is very grateful for helpful exchanges with Prof. C.A. Mayhew at the University of Innsbruck, Austria. The experimental work was supported by the National Natural Science Foundation of China (Grant Nos. 22241304, 22225303), the National Natural Science Foundation of China (NSFC Center for Chemical Dynamics (Grant No. 22288201)), the Scientific Instrument Developing Project of the Chinese Academy of Sciences (Grant No. GJJSTD20220001), the Innovation Program for Quantum Science and Technology (2021ZD0303304), the Innovation Fund Project of Dalian Institute of Chemical Physics (DICP I202112). X.Y. also thanks the Guangdong Science and Technology Program (Grant Nos. 2019ZT08L455 and 2019JC01X091), and the Shenzhen Science and Technology Program (Grant No. ZDSYS20200421111001787).

■ REFERENCES

(1) Eberhardt, P.; Meier, R.; Krankowsky, D.; Hodges, R. R. Methanol and Hydrogen Sulfide in Comet P/Halley. *Astron. Astrophys.* **1994**, *288*, 315−329.

(2) Bockelee-Morvan, D.; Lis, D. C.; Wink, J. E.; Despois, D.; Crovisier, J.; Bachiller, R.; Benford, D. J.; Biver, N.; Colom, P.; Davies, J. K.; et al. New Molecules Found in Comet C/1995 O1 (Hale-Bopp): Investigating the Link between Cometary and Interstellar Material. *Astron. Astrophys.* **2000**, *353*, 1101−1114.

(3) Boissier, J.; Bockelee-Morvan, D.; Biver, N.; Crovisier, J.; Despois, D.; Marsden, B. G.; Moreno, R. Interferometric Imaging of the Sulfur-bearing Molecules H_2S, SO, and CS in Comet C/1995 O1 (Hale-Bopp). *Astron. Astrophys.* **2007**, *475*, 1131−1144.

(4) Biver, N.; Bockelée-Morvan, D.; Moreno, R.; Crovisier, J.; Colom, P.; Lis, D. C.; Sandqvist, A.; Boissier, J.; Despois, D.; Milam, S. N. Ethyl Alcohol and Sugar in Comet C/2014 Q2 (Lovejoy). *Sci. Adv.* **2015**, *1*, No. e1500863.

(5) Calmonte, U.; Altwegg, K.; Balsiger, H.; Berthelier, J. J.; Bieler, A.; Cessateur, G.; Dhooghe, F.; van Dishoeck, E. F.; Fiethe, B.; Fuselier, S. A.; et al. Sulphur-bearing Species in the Coma of Comet 67P/Churyumov-Gerasimenko. *Mon. Not. R. Astron. Soc.* **2016**, *462*, S253−S273.

(6) Niemann, H. B.; Atreya, S. K.; Carignan, G. R.; Donahue, T. M.; Haberman, J. A.; Harpold, D. N.; Hartle, R. E.; Hunten, D. M.; Kasprzak, W. T.; Mahaffy, P. R.; et al. The Composition of the Jovian Atmosphere as Determined by the Galileo Probe Mass Spectrometer. *J. Geophys. Res. Planets* **1998**, *103*, 22831−22845.

(7) Irwin, P. G. J.; Toledo, D.; Garland, R.; Teanby, N. A.; Fletcher, L. N.; Orton, G. S.; Bezard, B. Detection of Hydrogen Sulfide above the Clouds in Uranus's Atmosphere. *Nat. Astron.* **2018**, *2*, 420−427.

(8) Molter, E. M.; de Pater, I.; Luszcz-Cook, S.; Tollefson, J.; Sault, R. J.; Butler, B.; de Boer, D. Tropospheric Composition and Circulation of Uranus with ALMA and the VLA. *Planetary Sci. J.* **2021**, *2*, 3.

(9) Irwin, P. G. J.; Toledo, D.; Garland, R.; Teanby, N. A.; Fletcher, L. N.; Orton, G. S.; Bezard, B. Probable Detection of Hydrogen Sulphide (H_2S) in Neptune's Atmosphere. *Icarus* **2019**, *321*, 550−563.

(10) Rivière-Marichalar, P.; Fuente, A.; Le Gal, R.; Arabhavi, A. M.; Cazaux, S.; Navarro-Almaida, D.; Ribas, A.; Mendigutía, I.; Barrado, D.; Montesinos, B. H_2S Observations in Young Stellar Disks in Taurus. *Astron. Astrophys.* **2021**, *652*, A46.

(11) Gorai, P.; Law, C. Y.; Tan, J. C.; Zhang, Y. C.; Fedriani, R.; Tanaka, T. E. I.; Bonfand, M.; Cosentino, G.; Mardones, D.; Beltrán, M. T.; et al. Astrochemical Diagnostics of the Isolated Massive Protostar G28.20−0.05. *Astrophys. J.* **2024**, *960*, 127.

(12) Tannock, M. E.; Metchev, S.; Hood, C. E.; Mace, G. N.; Fortney, J. J.; Morley, C. V.; Jaffe, D. T.; Lupu, R. A 1.46−2.48 μm Spectroscopic Atlas of a T6 Dwarf (1060 K) Atmosphere with IGRINS: First Detections of H_2S and H_2, and Verification of H_2O, CH_4, and NH_3 Line Lists. *Mon. Not. R. Astron. Soc.* **2022**, *514*, 3160−3178.

(13) Tsai, S. M.; Lee, E. K. H.; Powell, D.; Gao, P.; Zhang, X.; Moses, J.; Hébrard, E.; Venot, O.; Parmentier, V.; Jordon, S.; et al. Photochemically Produced SO_2 in the Atmosphere of WASP-39b. *Nature* **2023**, *617*, 483−487.

(14) Fu, G. W.; Welbanks, L.; Deming, D.; Inglis, J.; Zhang, M.; Lothringer, J.; Ih, J.; Moses, J. I.; Schlawin, E.; Knutson, H. A.; et al. Hydrogen Sulfide and Metal-Enriched Atmosphere for a Jupiter-Mass Exoplanet. *Nature* **2024**, *632*, 752−756.

(15) Vastel, C.; Phillips, T. G.; Ceccarelli, C.; Pearson, J. First Detection of Doubly Deuterated Hydrogen Sulfide. *Astrophys. J.* **2003**, *593*, L97−L100.

(16) Caselli, P.; Ceccarelli, C. Our Astrochemical Heritage. *Astron. Astrophys. Rev.* **2012**, *20*, 56.

(17) Ceccarelli, C. Spiers Lecture: Astrochemistry at High Resolution. *Farad. Disc.* **2023**, *245*, 11−51.

(18) Lee, L. C.; Wang, X. Y.; Suto, M. Quantitative Photoabsorption and Fluorescence Spectroscopy of H_2S and D_2S at 49−240 nm. *J. Chem. Phys.* **1987**, *86*, 4353−4361.
(19) Morley, G. P.; Lambert, I. D.; Mordaunt, D. H.; Wilson, S. H. S.; Ashfold, M. N. R.; Dixon, R. N.; Western, C. M. Translational Spectroscopy of H(D) Atom Fragments Arising from the Photodissociation of H_2S (D_2S): A Redetermination of D_0(SH). *J. Chem. Soc., Faraday Trans.* **1993**, *89*, 3865−3876.
(20) Gao, Q.; Chen, J. J.; Hu, X. X.; Xie, D. Q. Theoretical Study on Photodissociation Dynamics of Vibrational Excited States of H_2S in the First Absorption Band. *Chin. J. Chem. Phys.* **2024**, *37*, 221−229.
(21) Chen, J. J.; Gao, Q.; Zhou, L. S.; Hu, X. X.; Xie, D. Q. Isotope Effects on State-to-State Photodissociation Dynamics of D_2S in its First Absorption Band. *J. Phys. Chem. A.* **2024**, *128*, 1892−1901.
(22) Price, W. C.; Teegan, J. P.; Walsh, A. D. The Far Ultra-Violet Spectra of the Hydrides and Deuterides of Sulphur, Selenium and Tellurium and of the Methyl Derivatives of Hydrogen Sulphide. *Proc. R. Soc. A* **1950**, *201*, 600−609.
(23) Masuko, H.; Morioka, Y.; Nakamura, M.; Ishiguro, E.; Sasanuma, M. Absorption Spectrum of the H_2S Molecule in the Vacuum Ultraviolet Region. *Can. J. Phys.* **1979**, *57*, 745−760.
(24) Mayhew, C. A.; Connerade, J. P.; Baig, M. A.; Ashfold, M. N. R.; Bayley, J. M.; Dixon, R. N.; Prince, J. D. High-resolution Studies of the Electronic Spectra of H_2S and D_2S. *J. Chem. Soc., Faraday Trans. 2* **1987**, *82* (2), 417−434.
(25) Ashfold, M. N. R.; Bayley, J. M.; Dixon, R. N.; Prince, J. D. Molecular Predissociation Dynamics Revealed through Multiphoton Ionization Spectroscopy, III. New $^1A_2$ and $^1B_1$ Rydberg States in H_2S and D_2S. *Chem. Phys.* **1985**, *98*, 289−313.
(26) Ashfold, M. N. R.; Hartree, W. S.; Salvato, A. V.; Tutcher, B.; Walker, A. A Reinvestigation of the Rydberg States of H_2S and D_2S by Two-photon Resonant Multiphoton Ionisation Spectroscopy. *J. Chem. Soc. Faraday Trans.* **1990**, *86*, 2027−2034.
(27) Gallo, A. R.; Innes, K. K. A $^1B_1$ Rydberg State of the H_2S Molecule. *J. Mol. Spectrosc.* **1975**, *54*, 472−474.
(28) Ashfold, M. N. R.; Dixon, R. N. Multiphoton Ionisation Spectroscopy of H_2S: A Reinvestigation of the $^1B_1$−$^1A_1$ Band at 139.1 nm. *Chem. Phys. Lett.* **1982**, *93*, 5−10.
(29) Zhou, J.; Zhao, Y.; Hansen, C. S.; Yang, J.; Chang, Y.; Yu, Y.; Cheng, G.; Chen, Z.; He, Z.; Yu, S.; Ding, H.; Zhang, W.; Wu, G.; Dai, D.; Western, C. M.; Ashfold, M. N. R.; Yuan, K.; Yang, X. Ultraviolet Photolysis of H_2S and its Implications for SH Radical Production in the Interstellar Medium. *Nat. Commun.* **2020**, *11*, 1547.
(30) Zhao, Y. R.; Chen, J. J.; Luo, Z. J.; Li, Z. X.; Yang, S. K.; Chang, Y.; An, F.; Chen, Z. C.; Yang, J. Y.; Wu, G. R.; et al. Photodissociation of H_2S: A New Pathway for the Production of Vibrationally Excited Molecular Hydrogen in the Interstellar Medium. *J. Phys. Chem. Letts.* **2022**, *13*, 9786−9792.
(31) Zhao, Y. R.; Chen, J. J.; Luo, Z. J.; Chang, Y.; Yang, J. Y.; Zhang, W. Q.; Wu, G. R.; Crane, S. W.; Hansen, C. S.; Ding, H. B.; et al. The Vibronic State Dependent Predissociation of H_2S: Determination of all Fragmentation Processes. *Chem. Sci.* **2023**, *14*, 2501−2517.
(32) Zhao, Y.; Luo, Z.; Chang, Y.; Wu, Y.; Zhang, S. E.; Li, Z.; Ding, H.; Wu, G.; Campbell, J. S.; Hansen, C. S.; Crane, S. W.; Western, C. M.; Ashfold, M. N. R.; Yuan, K.; Yang, X. Rotational and Nuclear-spin Level Dependent Photodissociation Dynamics of H_2S. *Nat. Commun.* **2021**, *12*, 4459.
(33) Luo, Z. J.; Wu, Y. C.; Yang, S. K.; Li, Z. X.; Hua, W.; Chen, Z. C.; Che, L.; Wang, X. G.; Ashfold, M. N. R.; Yuan, K. J. Unraveling the Rich Fragmentation Dynamics Associated with S−H Bond Fission Following Photoexcitation of H_2S at Wavelengths ∼ 129.1 nm. *J. Phys. Chem. A.* **2024**, *128*, 3351−3360.
(34) Wheeler, M. D.; Orr-Ewing, A. J.; Ashfold, M. N. R. Predissociation Dynamics of the $A^2\Sigma^+$ State of SH and SD. *J. Chem. Phys.* **1997**, *107*, 7591−7600.
(35) Rose, R. A.; Orr-Ewing, A. J.; Yang, C. H.; Vidma, K.; Groenenboom, G. C.; Parker, D. H. Photodissociation Dynamics of the $A^2\Sigma^+$ State of SH and SD Radicals. *J. Chem. Phys.* **2009**, *130*, No. 034307.
(36) Qin, Y.; Zheng, X.; Song, Y.; Sun, G.; Zhang, J. Vibrational Energy Levels and Predissociation Lifetimes of the $A^2\Sigma^+$ State of SH/SD Radicals by Photodissociation Spectroscopy. *J. Chem. Phys.* **2022**, *157*, 134303.
(37) Qin, Y.; Zheng, X. F.; Song, Y.; Sun, G.; Zhang, J. S. Two-Photon Dissociation Dynamics of the Mercapto Radical. *Phys. Chem. Chem. Phys.* **2022**, *24*, 27232−27240.
(38) Cook, P. A.; Langford, S. R.; Dixon, R. N.; Ashfold, M. N. R. An Experimental and Ab Initio Reinvestigation of the Lyman-α Photodissociation of H_2S and D_2S. *J. Chem. Phys.* **2001**, *114*, 1672−1684.
(39) Kreis, C.; Hollenstein, U.; Merkt, F. Threshold Ion-Pair-Production Spectroscopy of H_2S and D_2S. *Mol. Phys.* **2022**, *120*, No. e2071349.
(40) Kramida, A.; Ralchenko, Y.; Reader, J. Atomic Spectroscopy Data. In *NIST Atomic Spectra Database*; National Institute of Standards and Technology: Gaithersburg, MD, 2019. https://www.nist.gov.
(41) Ramsay, D. A. Absorption Spectra of SH and SD Produced by Flash Photolysis of H_2S and D_2S. *J. Chem. Phys.* **1952**, *20*, 1920−1927.
(42) Lai, K. F.; Beyer, M.; Ubachs, W. Spectroscopic Study of the $F^1\Sigma^+_g$ Outer Well State in H_2, HD and D_2. *J. Mol. Spectrosc.* **2023**, *393*, No. 111778.
(43) Ashfold, M. N. R.; Yuan, K.; Yang, X. Perspective: The Development and Applications of H Rydberg Atom Translational Spectroscopy Methods. *J. Chem. Phys.* **2018**, *149*, No. 080901.
(44) Chang, Y.; Zhou, J. M.; Luo, Z. J.; Chen, Z. C.; He, Z. G.; Yu, S. R.; Che, L.; Wu, G. R.; Wang, X. A.; Yuan, K. J.; et al. Photodissociation Dynamics of H_2O and D_2O via the $\tilde{D}(^1A_1)$ Electronic State. *Phys. Chem. Chem. Phys.* **2020**, *22*, 4379−4386.
(45) Luo, Z.; Zhao, Y.; Chen, Z.; Chang, Y.; Zhang, S. E.; Wu, Y.; Yang, J.; Cheng, Y.; Che, L.; Wu, G.; Xie, D.; Yang, X.; Yuan, K. Strong Isotope Effect in the VUV Photodissociation of HOD: A Possible Origin of D/H Isotope Heterogeneity in the Solar Nebula. *Sci. Adv.* **2021**, *7*, No. eabg7775.
(46) Chang, Y.; Yu, Y.; An, F.; Luo, Z.; Quan, D.; Zhang, X.; Hu, X.; Li, Q.; Yang, J.; Chen, Z.; Che, L.; Zhang, W.; Wu, G.; Xie, D.; Ashfold, M. N. R.; Yuan, K.; Yang, X. Three Body Photodissociation of the Water Molecule and Its Implications for Prebiotic Oxygen Production. *Nat. Commun.* **2021**, *12*, 2476.
(47) Chang, Y.; Yu, Y.; Wang, H.; Hu, X.; Li, Q.; Yang, J.; Su, S.; He, Z.; Chen, Z.; Che, L.; Wang, X.; Zhang, W.; Wu, G.; Xie, D.; Ashfold, M. N. R.; Yuan, K.; Yang, X. Hydroxyl Super Rotors from Vacuum Ultraviolet Photodissociation of Water. *Nat. Commun.* **2019**, *10*, 1250.
(48) Chang, Y.; Ashfold, M. N. R.; Yuan, K.; Yang, X. Exploring the Vacuum Ultraviolet Photochemistry of Astrochemically Important Triatomic Molecules. *Natl. Sci. Rev.* **2023**, *10*, nwad158.
(49) Chang, Y.; He, Z. G.; Luo, Z. J.; Zhou, J. M.; Zhang, Z. G.; Chen, Z. C.; Yang, J. Y.; Yu, Y.; Li, Q. M.; Che, L.; et al. Application of Laser Dispersion Method in Apparatus Combining H Atom Rydberg Tagging Time-of-Flight Technique with Vacuum Ultraviolet Free Electron Laser. *Chin. J. Chem. Phys.* **2020**, *33*, 139−144.
(50) Western, C. M. PGOPHER: A Program for Simulating Rotational, Vibrational and Electronic Spectra. *J. Quant. Spectrosc. Radiat. Transf.* **2017**, *186*, 221−242.
(51) Miller, R. E.; Leroi, G. E.; Hard, T. M. Analysis of the Pure Rotational Absorption Spectra of Hydrogen Sulfide and Deuterium Sulfide. *J. Chem. Phys.* **1969**, *50*, 677−684.
(52) Duxbury, G.; Horani, M.; Rostas, J. Rotational Analysis of Electronic Emission-Spectrum of H_2S^+ Ion Radical. *Proc. R. Soc. A* **1972**, *331*, 109−137.
(53) Yuan, K. J.; Cheng, Y.; Cheng, L.; Guo, Q.; Dai, D. X.; Wang, X. Y.; Yang, X. M.; Dixon, R. N. Nonadiabatic Dissociation Dynamics in H_2O: Competition between Rotationally and Non-Rotationally Mediated Pathways. *Proc. Nat. Acad. Sci.* **2008**, *105*, 19148−19153.

https://doi.org/10.1021/acs.jpca.4c04730
J. Phys. Chem. A XXXX, XXX, XXX−XXX

(54) Yuan, K. J.; Dixon, R. N.; Yang, X. M. Photochemistry of the Water Molecules: Adiabatic versus Nonadiabatic Dynamics. *Acc. Chem. Res.* **2011**, *44*, 369−378.
(55) Connerade, J. P.; Baig, M. A.; Mayhew, C. A.; Hormes, J. Synchrotron Spectroscopy of Molecules at High Resolution. *J. Electron Spectrosc. Relat. Phenom.* **1995**, *73*, 173−190.
(56) Mayhew, C. A. The High Resolution Vacuum Ultraviolet Absorption Spectra of the Group VI Dihydrides and Deuterides. Ph. D. Thesis, University of London, 1985.
(57) Camy-Peyret, C.; Flaud, J. M.; N'Gom, A.; Johns, J. W. C. The Three Fundamental Bands, ν_2, ν_1 and ν_3 of $D_2{}^{32}S$ and the ν_2 Band of $D_2{}^{34}S$. *Mol. Phys.* **1988**, *65*, 649−657.
(58) Chang, Y.; Chen, Z. C.; Zhou, J.; Luo, Z. J.; He, Z. G.; Wu, G. R.; Ashfold, M. N. R.; Yuan, K. J.; Yang, X. M. Striking Isotopologue-Dependent Photodissociation Dynamics of Water Molecules: The Signature of an Accidental Resonance. *J. Phys. Chem. Letts.* **2019**, *10*, 4209−4214.

https://doi.org/10.1021/acs.jpca.4c04730
J. Phys. Chem. A XXXX, XXX, XXX−XXX